

Supporting Information

Multiple-resonance thermally activated delayed fluorescence materials based on phosphorus central chirality for efficient circularly polarized electroluminescence

Yu Wang, Zi-Yi Lv, Zi-Xuan Chen, Shuai Xing, Zhong-Zhong Huo, Xian-Fang Hong, Li Yuan, Wei Li, and You-Xuan Zheng*

^a State Key Laboratory of Coordination Chemistry, Jiangsu Key Laboratory of Advanced Organic Materials, School of Chemistry and Chemical Engineering, Nanjing University. Nanjing 210023, P. R. China, E-mail: yxzheng@nju.edu.cn

S1. General Information

All solvents and reagents were commercially available without further purification. NMR measurements were conducted on a Bruker AM 400 spectrometer. High-resolution mass spectra were recorded on a MICROTOF-Q III instrument. Absorption and emission spectra were measured on a UV-3100 and a Hitachi F-4600 photoluminescence spectrophotometer, respectively. Electrochemical measurements were conducted on an AUTOLAB-CV-75W analyzer with a scan rate of 100 mV/s. The electrochemical cell was a standard three-compartment cell composed of a glass carbon working electrode, a Pt auxiliary electrode, and a Pt wire reference electrode. All tests were performed using [Bu₄N][PF₆] (0.1 M) as the supporting electrolyte. The voltammograms were obtained in anhydrous and nitrogen saturated CH₂Cl₂ solutions. The potentials are reported relative to the ferrocene/ferrocenium couple. The absolute photoluminescence quantum yields of the compounds were measured with HORIBA FL-3 fluorescence spectrometer. The decay lifetimes of the compounds were measured with Edinburgh FLS980 fluorescence spectrometer. Fluorescence lifetime testing, using an FPGA based TDC-TCSPC module (MODEL: FF4, Orient KOJI Ltd., Tianjin, CHN), coupled with a pulse 355 nm laser output of 1 kHz, can achieve uninterrupted testing from 100 ps⁻¹ ms. At the same time, in logarithmic abscissa mode, it is easy to collect the decay curve in the full time domain and use it for photon number statistics. CPL and CPEL spectra were performed with a JASCO CPL-300 spectrometer. Thermogravimetric analysis measurements were performed on a Pyris 1 DSC under nitrogen at a heating rate of 10 °C min⁻¹. The ground state geometries are based on single crystal structure, electron cloud distributions were calculated using Gaussian 09 software¹ by density functional theory (DFT) using the M062X functional with the 6-31G(d) basis set. Time-dependent DFT (TD-DFT) with PBE0 functional with the 6-31G(d, p) basis set. The input files and orbital representations were generated with Multiwfn² (isovalue = 0.03). X-ray single crystals were obtained on a Bruker D8 X-ray single crystal Venture diffractometer using CuK α radiation ($\lambda = 1.54178$) at 180K for all compounds. SAINT5.0 and SADABS programs are used for the reduction and absorption correction of crystal data. The resolution and refinement of the crystal

structure are obtained on the SHELXTL-97 software, using the direct or Patterson methods. All non-hydrogen source coordinates are obtained by using the differential Fourier method and the least square method. Then the geometric method and the difference value are used. The hydrogen atom coordinates were obtained by Fourier method, and the crystal structure was obtained. The rate constants of intersystem crossing (k_{ISC}) and reverse intersystem crossing (k_{RISC}) were calculated from the following six equations:

$$k_p = 1/\tau_p \dots \dots \dots \text{Eq.(1)}$$

$$k_d = 1/\tau_d \dots \dots \dots \text{Eq.(2)}$$

$$k_{r,s} = \Phi_p k_p + \Phi_d k_d \approx \Phi_p k_p \dots \dots \dots \text{Eq.(3)}$$

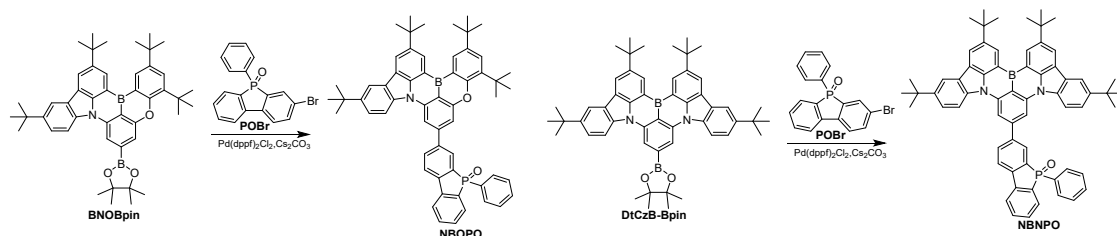
$$k_{nr,s} = \frac{1 - \Phi_{PL}}{\Phi_{PL}} k_{r,s} \dots \dots \dots \text{Eq.(4)}$$

$$k_{ISC} = k_p - k_{r,s} - k_{nr} \dots \dots \dots \text{Eq.(5)}$$

$$k_{RISC} = (k_p k_d \Phi_d) / (k_{ISC} \Phi_p) \dots \dots \dots \text{Eq.(6)}$$

The τ_p and τ_d represent the prompt and decay fluorescence lifetimes, respectively, which were determined from transient PL spectra. The k_p and k_d represent the decay rate constants for prompt and delayed fluorescence, respectively. Φ_p and Φ_d indicate prompt and delayed fluorescence components and can be distinguished from the total Φ_{PL} by comparing the integrated intensities of prompt and delayed components in the transient PL spectra.

S2. Experiment section



Scheme S1. Synthetic procedure of NBOPO and NBNPO

Compounds DtCzB-Bpin³, BNOBpin⁴, POBr⁵ were synthesized according to previously reported procedures.

Synthesis of NBOPO. The mixture of BNOBpin (0.52 g, 0.75 mmol), POBr (0.18 g, 0.50 mmol), Pd(dppf)Cl₂ (0.04 g, 0.05 mmol), Cs₂CO₃ (0.49 g, 1.50 mmol) in THF/water (50 mL/10 mL) was heated at 75 °C for 24 hours under nitrogen. After cooling to RT, the solvent was removed under reduced pressure and the residue was dissolved in H₂O (30 mL) and extracted with CH₂Cl₂. Then the organic layer was dried over Na₂SO₄. CH₂Cl₂ was evaporated under reduced pressure. The crude product was purified with chromatography on silica using PE/EA (5/1, v/v) as eluent to give yellow solid. Yield: 0.20 g, 48%. ¹H NMR (400 MHz, Methylene CD₂Cl₂) δ 9.01 (d, *J* = 1.9 Hz, 1H), 8.80 (d, *J* = 2.4 Hz, 1H), 8.53 (d, *J* = 1.8 Hz, 1H), 8.41 (d, *J* = 1.3 Hz, 1H), 8.37 (d, *J* = 8.8 Hz, 1H), 8.31 (d, *J* = 2.0 Hz, 1H), 8.22 (dd, *J* = 10.2, 1.7 Hz, 1H), 8.17 (dt, *J* = 8.1, 1.5 Hz, 1H), 8.09 (dd, *J* = 8.0, 3.0 Hz, 1H), 7.98 (dd, *J* = 7.8, 2.9 Hz, 1H), 7.83 (d, *J* = 2.4 Hz, 1H), 7.81 – 7.65 (m, 5H), 7.63 (d, *J* = 1.2 Hz, 1H), 7.56 – 7.36 (m, 4H), 1.68 (s, 9H), 1.63 (s, 9H), 1.53 (d, *J* = 2.5 Hz, 18H). ¹³C NMR (101 MHz, CD₂Cl₂) δ 159.48, 156.82, 146.12, 146.06, 145.43, 144.91, 143.12, 142.98, 142.87, 142.68, 142.14, 141.92, 141.87, 141.66, 138.37, 137.98, 135.21, 134.34, 134.17, 133.94, 133.32, 132.66, 132.64, 132.16, 131.47, 131.36, 131.13, 130.22, 130.17, 130.12, 130.05, 129.36, 129.27, 129.18, 129.14, 129.11, 127.20, 125.22, 124.45, 122.47, 122.36, 122.10, 122.01, 121.65, 117.78, 114.27, 107.88, 106.35, 35.82, 35.51, 35.15, 35.09, 32.28, 31.95, 31.82, 30.64, 27.34. ESI-MS. Calcd. for C₅₈H₅₈BNO₂P⁺([M+H])⁺: *m/z* 842.4293. Found: *m/z* 842.4290.

Synthesis of NBNPO. The mixture of DtCzB-Bpin (0.58 g, 0.75 mmol), POBr (0.18 g, 0.50 mmol), Pd(dppf)Cl₂ (0.04 g, 0.05 mmol), Cs₂CO₃ (0.49 g, 1.50 mmol) in THF/water (50 mL/10 mL) was heated at 75 °C for 22 hours under nitrogen. After cooling to RT, the solvent was removed under reduced pressure and the residue was dissolved in H₂O (30 mL) and extracted with CH₂Cl₂. Then the organic layer was dried over Na₂SO₄. CH₂Cl₂ was evaporated under reduced pressure. The crude product was purified with chromatography on silica using PE/EA (5/1, v/v) as eluent to give yellow solid. Yield: 0.26 g, 57%. ¹H NMR (400 MHz, CDCl₃) δ 9.09 (d, *J* = 1.9 Hz, 2H), 8.51 – 8.41 (m, 4H), 8.35 (d, *J* = 8.8 Hz, 2H), 8.28 – 8.19 (m, 3H), 8.15 – 8.02 (m, 2H), 7.94 (dd, *J* = 8.0, 2.6 Hz, 1H), 7.88 – 7.73 (m, 3H), 7.71 – 7.62 (m, 3H), 7.55 – 7.37 (m, 4H),

1.67 (s, 18H), 1.53 (s, 18H). ^{13}C NMR (101 MHz, CDCl_3) δ 145.60, 144.89, 144.77, 143.59, 143.49, 141.84, 141.57, 138.34, 134.75, 133.74, 133.29, 132.45, 131.32, 131.21, 130.46, 130.28, 130.19, 129.89, 129.38, 129.28, 129.06, 128.94, 127.24, 124.87, 123.83, 122.54, 122.16, 121.76, 121.64, 121.55, 120.88, 117.43, 114.29, 106.97, 35.32, 34.96, 32.33, 31.97, 29.86, 22.85, 14.27, 1.18. ESI-MS. Calcd. for $\text{C}_{64}\text{H}_{61}\text{BN}_2\text{OP}^+([\text{M}+\text{H}]^+)$: m/z 915.4609. Found: m/z 915.4607.

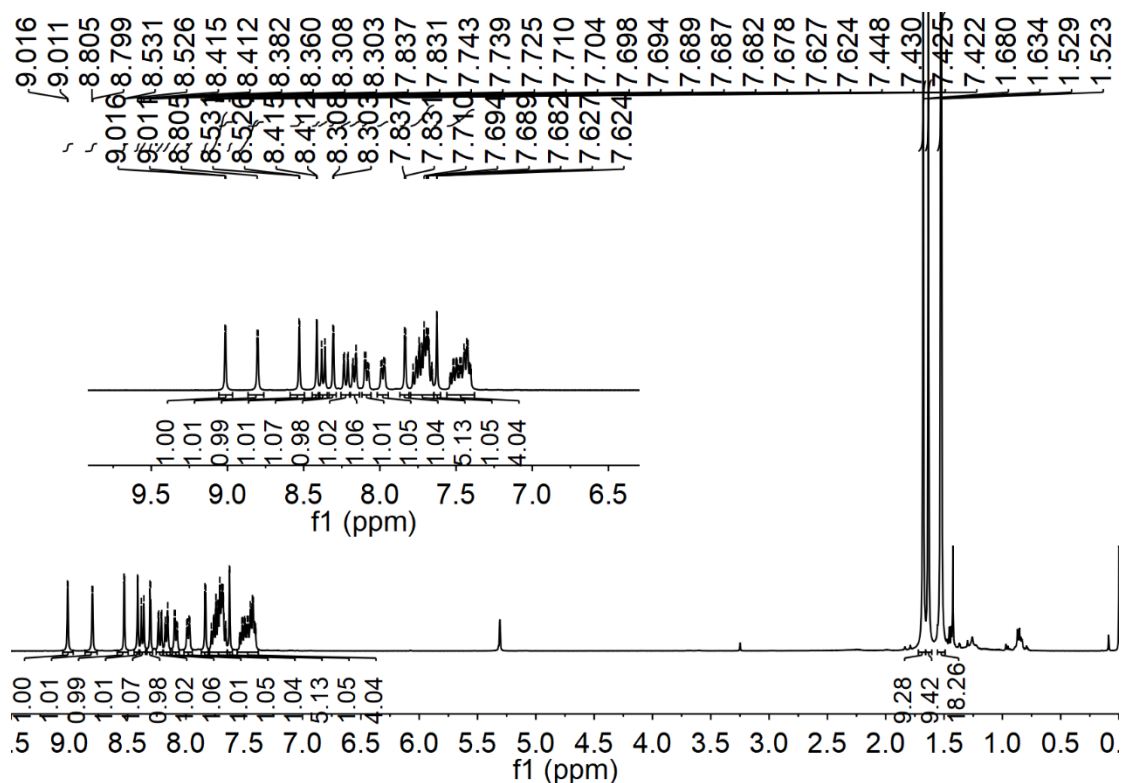


Figure S1. ^1H NMR (400 MHz, CD_2Cl_2) spectrum of NBOPO.

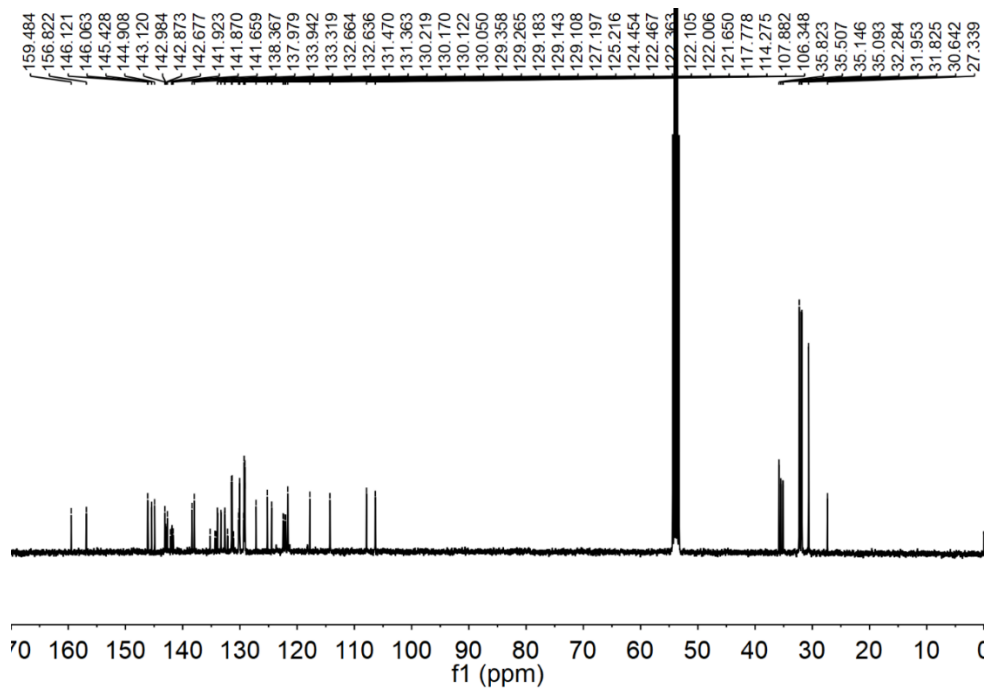


Figure S2. ^{13}C NMR (101 MHz, CD_2Cl_2) spectrum of NBOPO.

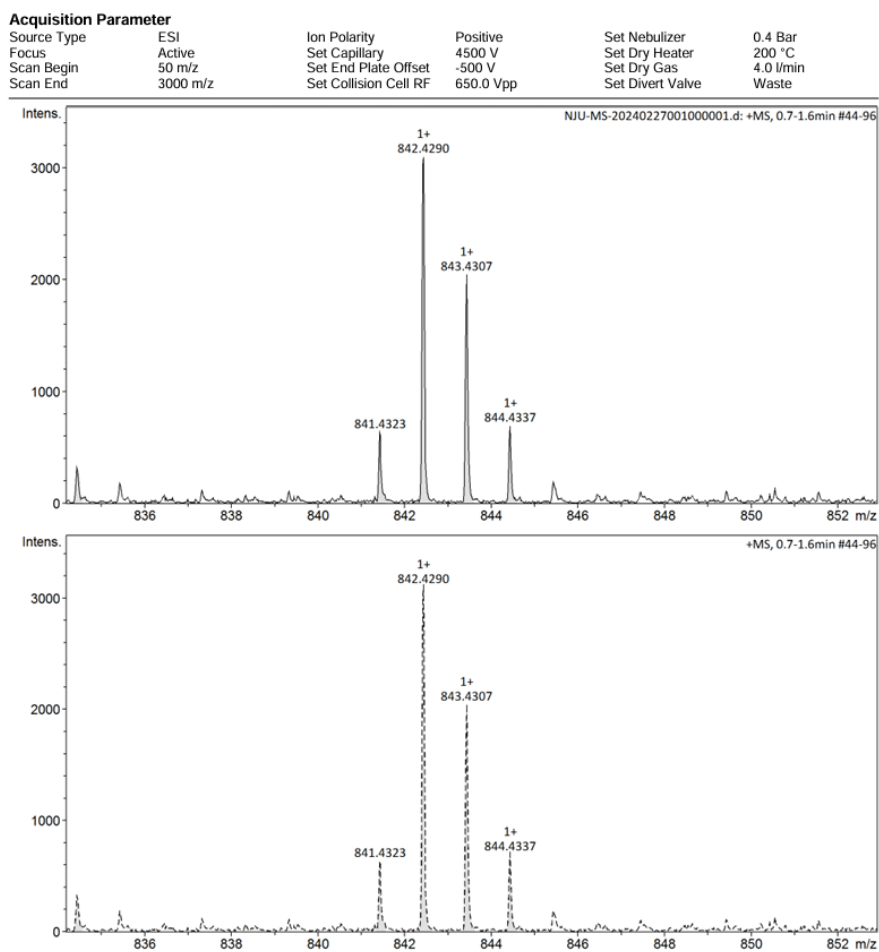


Figure S3. HRMS spectrum for NBOPO.

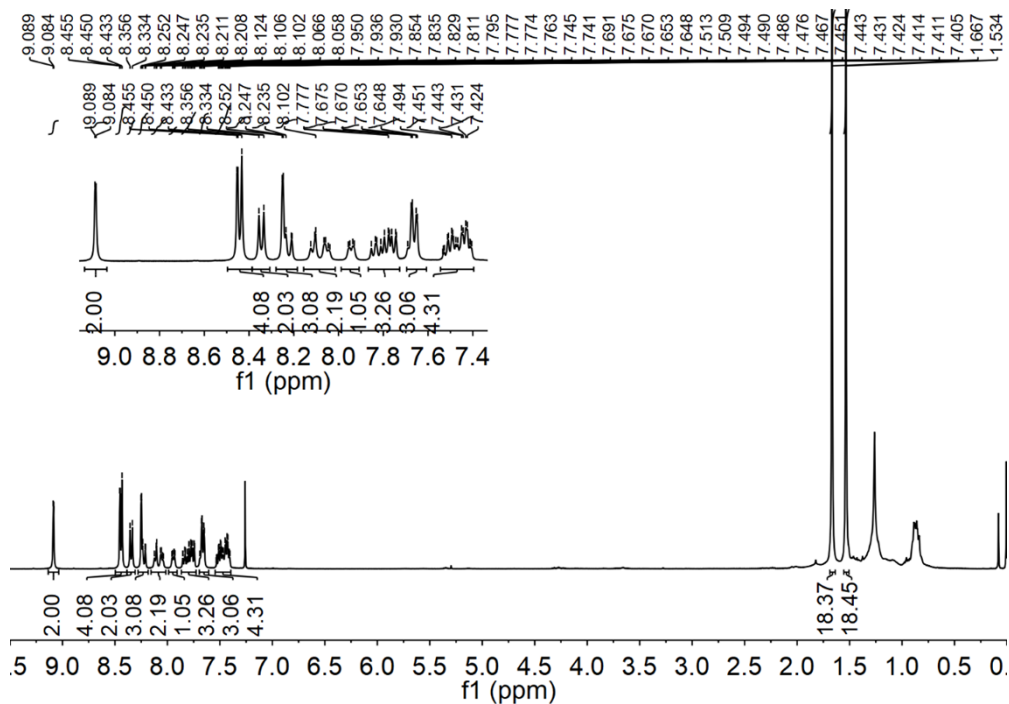


Figure S4. ^1H NMR (400 MHz, CDCl_3) spectrum of NBNPO.

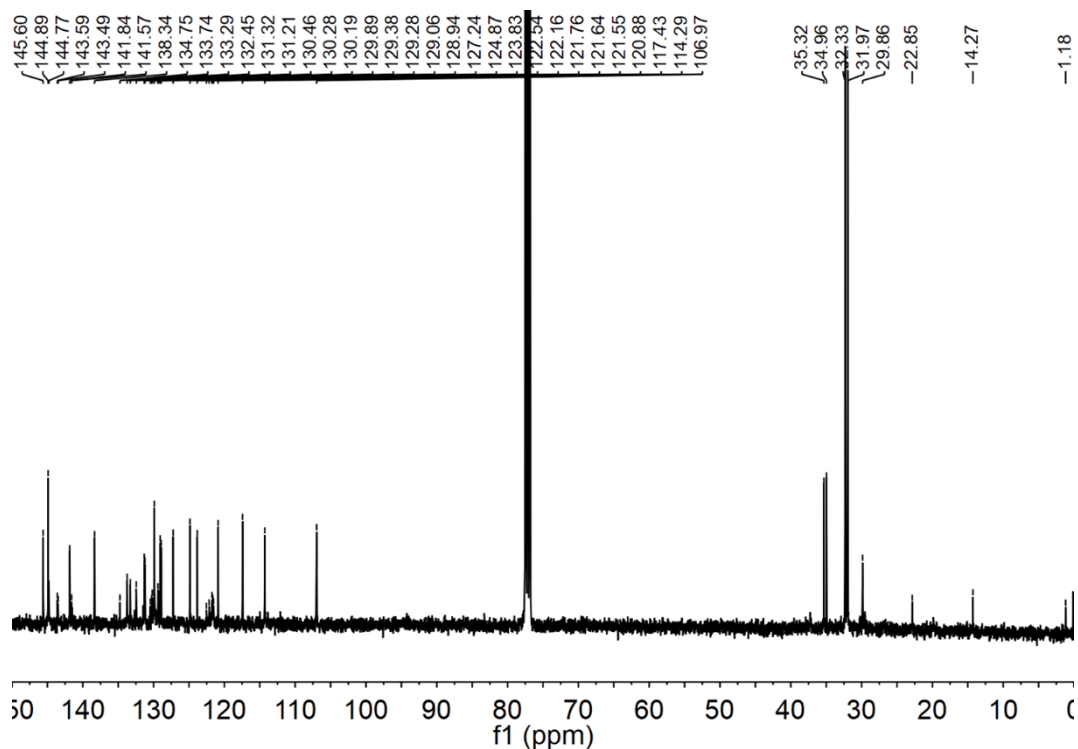


Figure S5. ^{13}C NMR (101 MHz, CDCl_3) spectrum of NBNPO.

Acquisition Parameter

Source Type	ESI	Ion Polarity	Positive	Set Nebulizer	0.4 Bar
Focus	Active	Set Capillary	4500 V	Set Dry Heater	200 °C
Scan Begin	50 m/z	Set End Plate Offset	-500 V	Set Dry Gas	4.0 l/min
Scan End	3000 m/z	Set Collision Cell RF	650.0 Vpp	Set Divert Valve	Waste

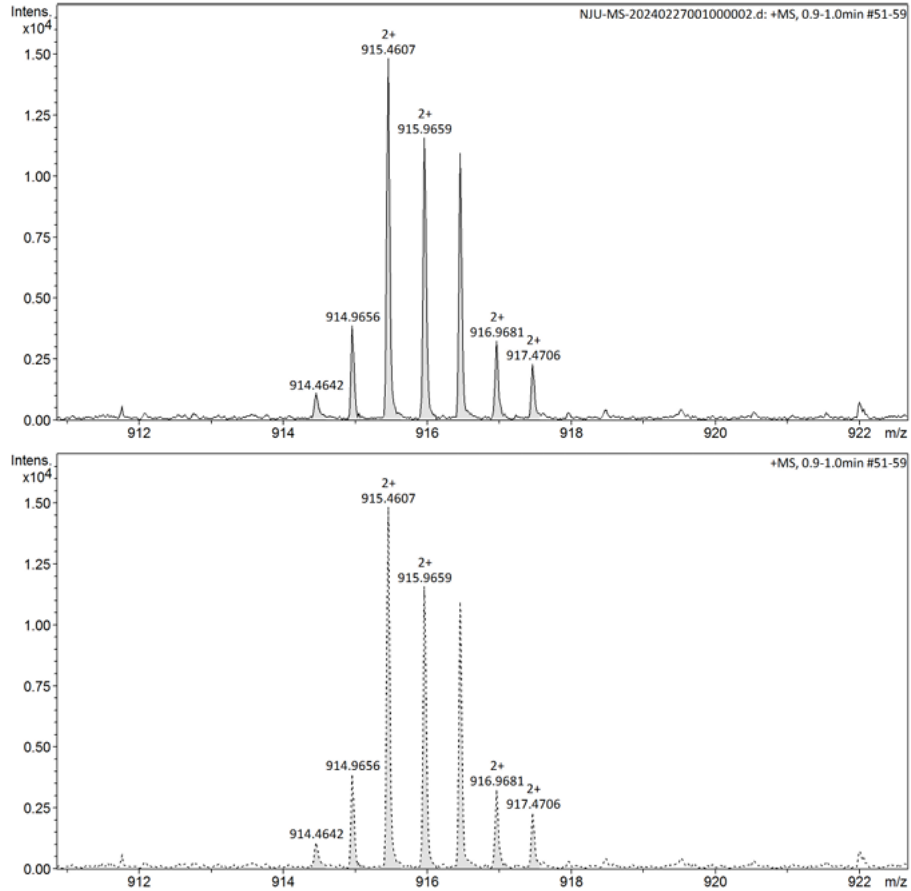
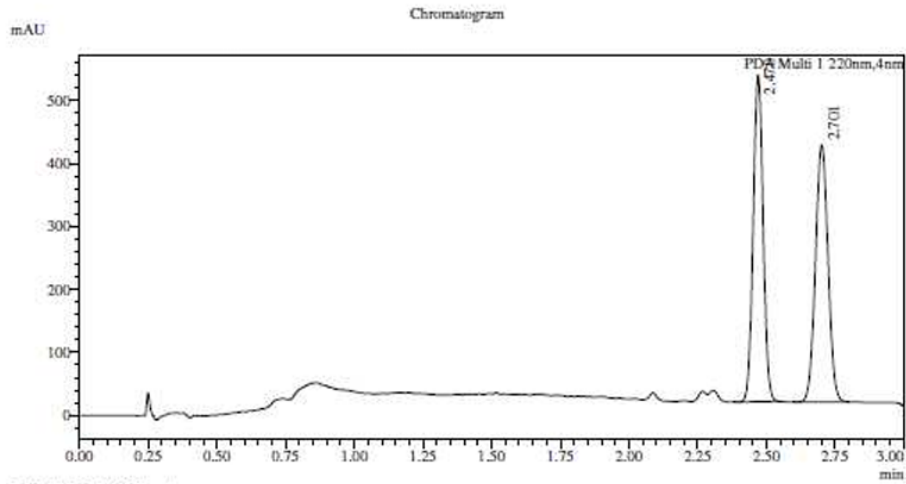


Figure S6. HRMS spectrum for NBNPO.



1 PDA Multi 1 / 220nm,4nm

Integration Result

Peak Table

Peak#	Ret. Time	Height	Height%	Resolution(USP)	Area	Area%
1	2.470	514438	55.885	--	1301872	50.036
2	2.701	406092	44.115	2.955	1299993	49.964

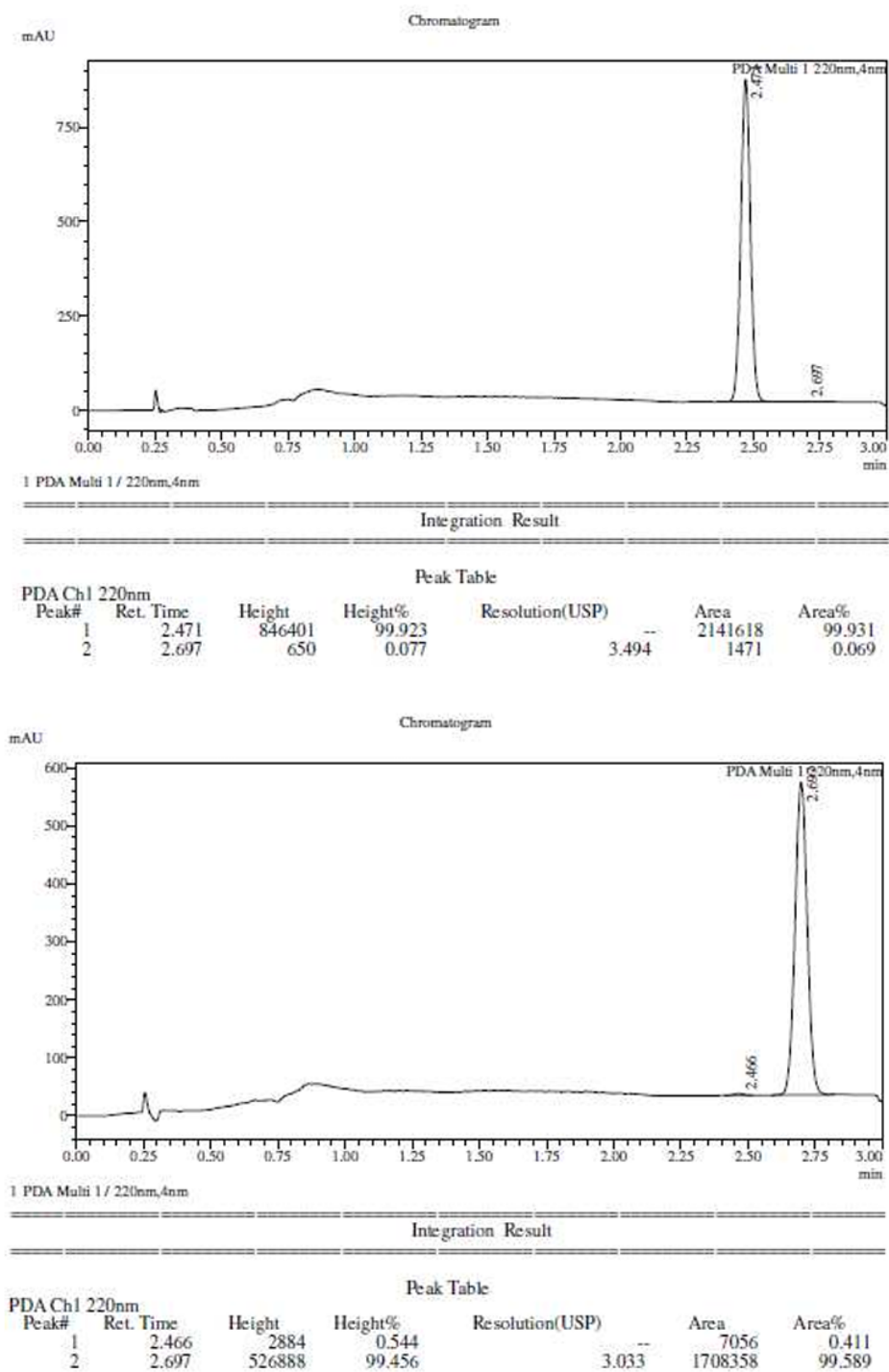


Figure S7. Chiral HPLC analysis of racemic **POBr** eluted by IPA (0.05% DEA) in CO₂ from 5% to 40% using Chiralpak AD-3 column (50*4.6 mm, 3 μm). Elution rate: 3 mL/min.

Table S1. Crystal data and structure refinement for (*S*)-NBOPO and (*S*)-NBNPO.

Parameter	(<i>S</i>)-NBOPO	(<i>S</i>)-NBNPO
CCDC No.	2344376	2344374
Empirical formula	C ₅₈ H ₅₇ BNO ₂ P	C ₆₄ H ₆₀ BN ₂ OP
Formula weight	841.42	914.45
Temperature/K	193.00	193.00
Crystal system	monoclinic	trigonal
Space group	<i>P</i> 2 ₁	<i>P</i> 3 ₂ 21
<i>a</i> /Å	9.2454(13)	32.7114(13)
<i>b</i> /Å	19.524(3)	32.7114(13)
<i>c</i> /Å	29.571(6)	23.7266(14)
<i>α</i> /°	90	90
<i>β</i> /°	92.763(7)	90
<i>γ</i> /°	90	120
Volume/Å ³	5331.5(15)	21987(2)
<i>Z</i>	2	12
$\rho_{\text{calc}}/\text{cm}^3$	1.181	0.829
μ/mm^{-1}	1.926	0.566
<i>F</i> (000)	2002.0	5832.0
Crystal size/mm ³	0.12 × 0.11 × 0.09	0.12 × 0.11 × 0.09
Radiation	CuK α (λ = 1.54178)	CuK α (λ =1.54178)
2 Θ range for data collection/°	5.426 to 136.48	3.118 to 137.428
Index ranges	-11 ≤ <i>h</i> ≤ 11, -23 ≤ <i>k</i> ≤ 23, -235 ≤ <i>l</i> ≤ 35	-39 ≤ <i>h</i> ≤ 21, -31 ≤ <i>k</i> ≤ 39, -22 ≤ <i>l</i> ≤ 28

Reflections collected	80238	147643
Independent reflections	18201 [Rint = 0.1205, Rsigma = 0.0988]	25876 [Rint = 0.0948, Rsigma = 0.0675]
Data/restraints/parameters	18201/275/1295	25876/1572/1312
Goodness-of-fit on F ²	1.030	1.005
Final R indexes [I>2σ (I)]	R1 = 0.0927, wR2 = 0.2468	R1 = 0.0834, wR2 = 0.2298
Final R indexes [all data]	R1 = 0.1386, wR2 = 0.2880	R1 = 0.1228, wR2 = 0.2811
Largest diff. peak/hole / e Å ⁻³	0.65/-0.34	0.27/-0.27
Flack parameter	0.052(13)	0.091(13)

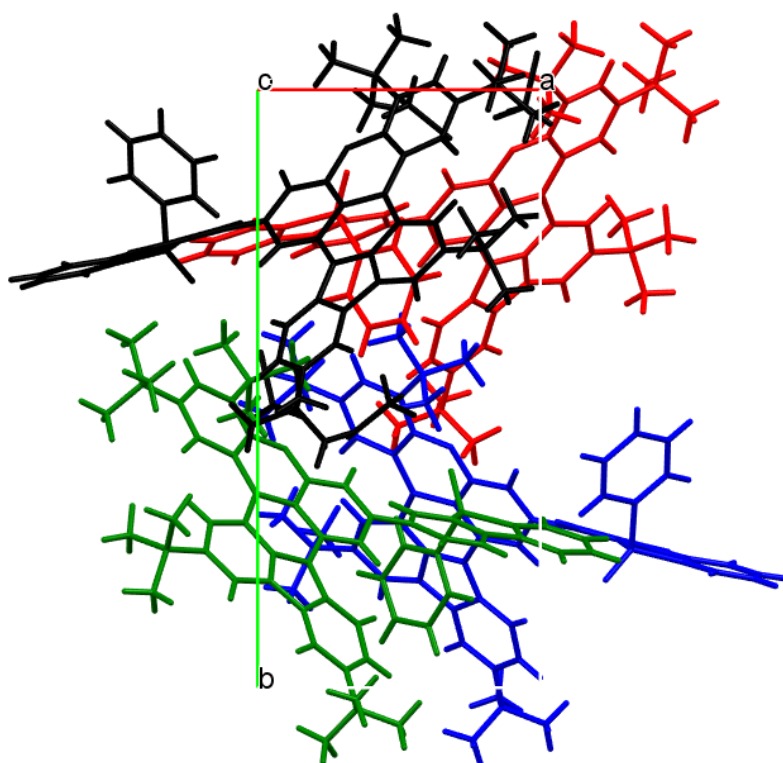


Figure S8. Packing mode of (*S*)-NBOPO alongside *c* axis.

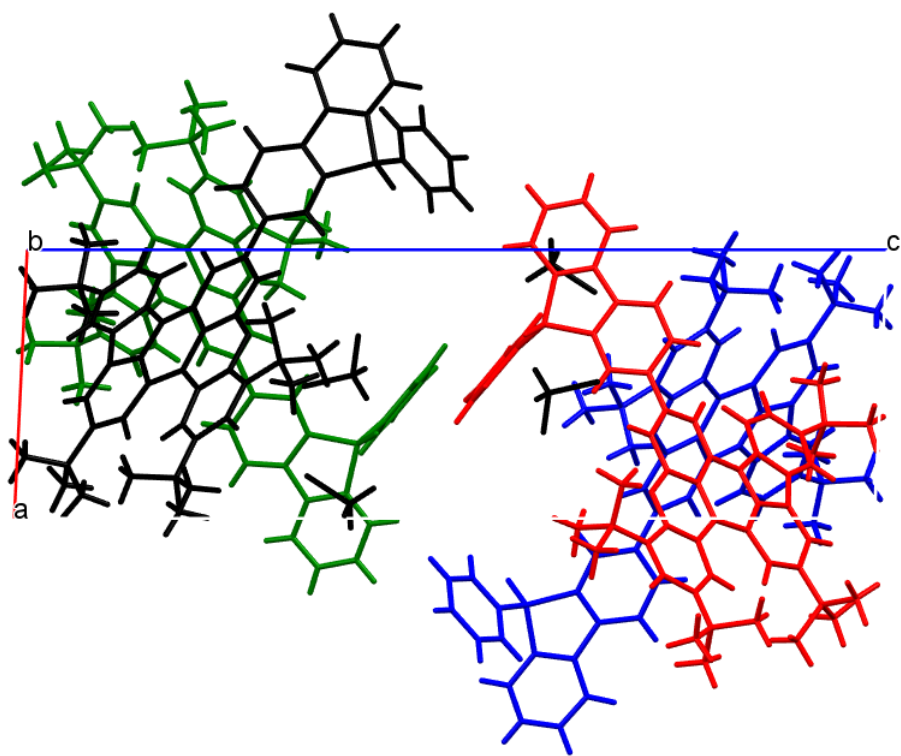


Figure S9. Packing mode of (*S*)-NBOPO alongside b axis.

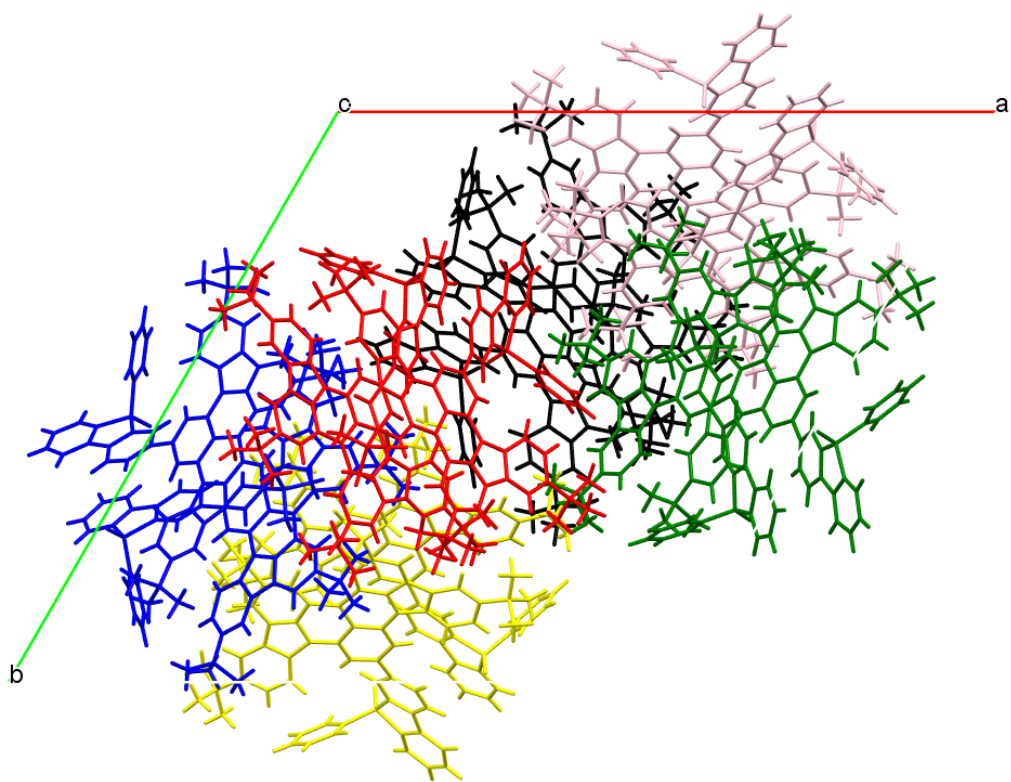


Figure S10. Packing mode of (*S*)-NBNPO alongside c axis.

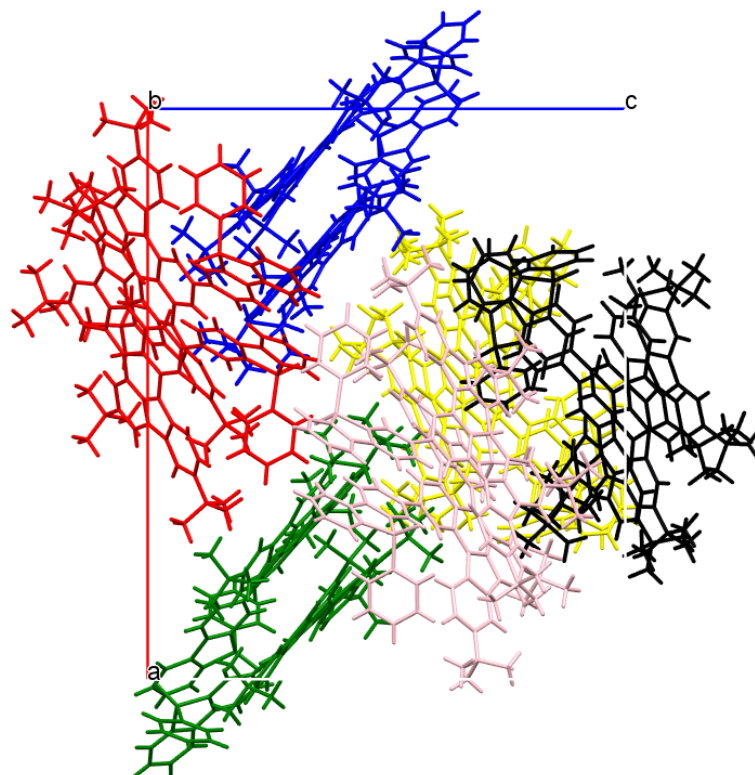


Figure S11. Packing mode of (*S*)-NBNPO alongside b axis.

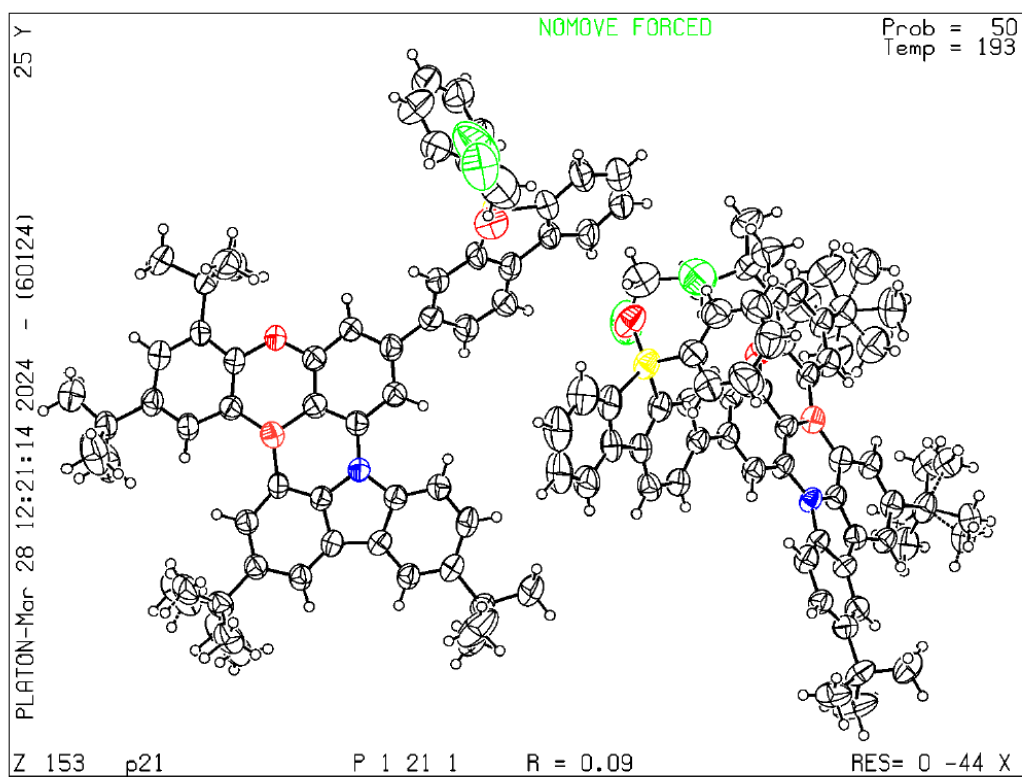


Figure S12. Crystal structure of (*S*)-NBOPO.

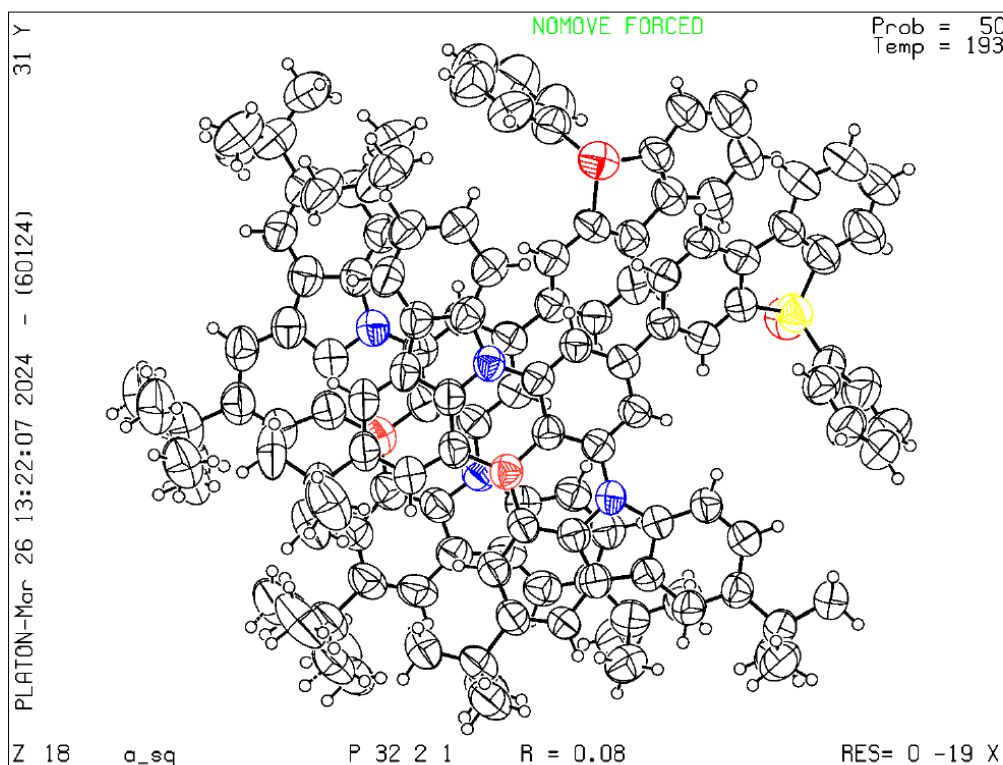


Figure S13. Crystal structure of (*S*)-NBNPO.

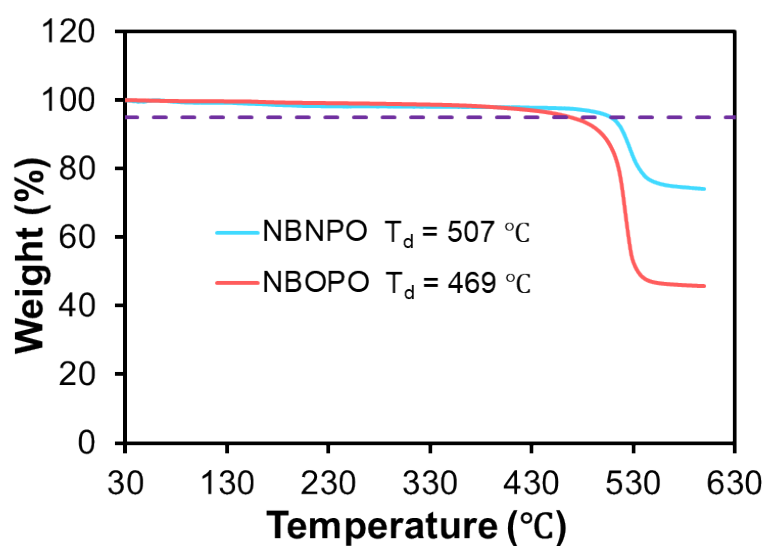


Figure S14. The TGA curves of NBOPO and NBNPO.

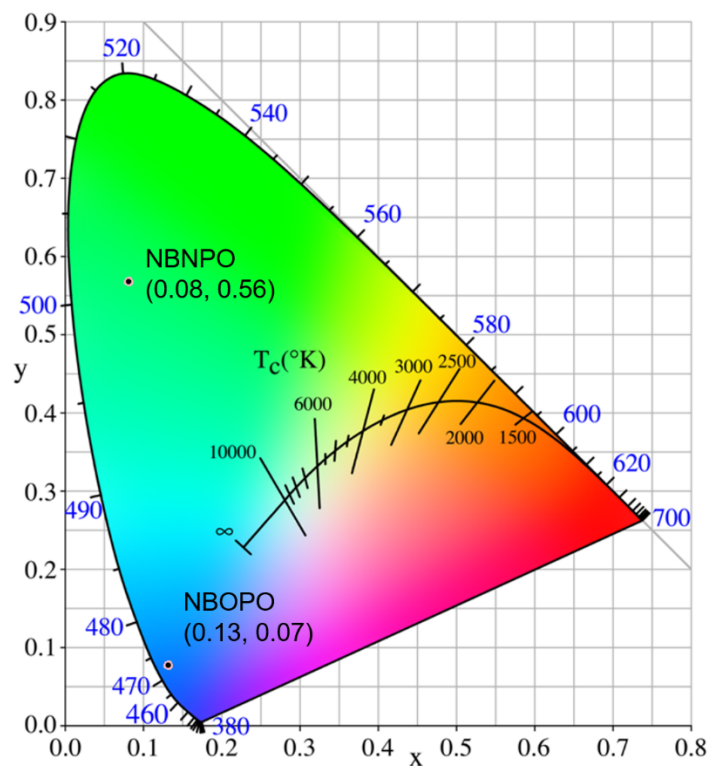


Figure S15. The corresponding CIE coordinates of NBOPO and NBNPO in toluene (3×10^{-5} M).

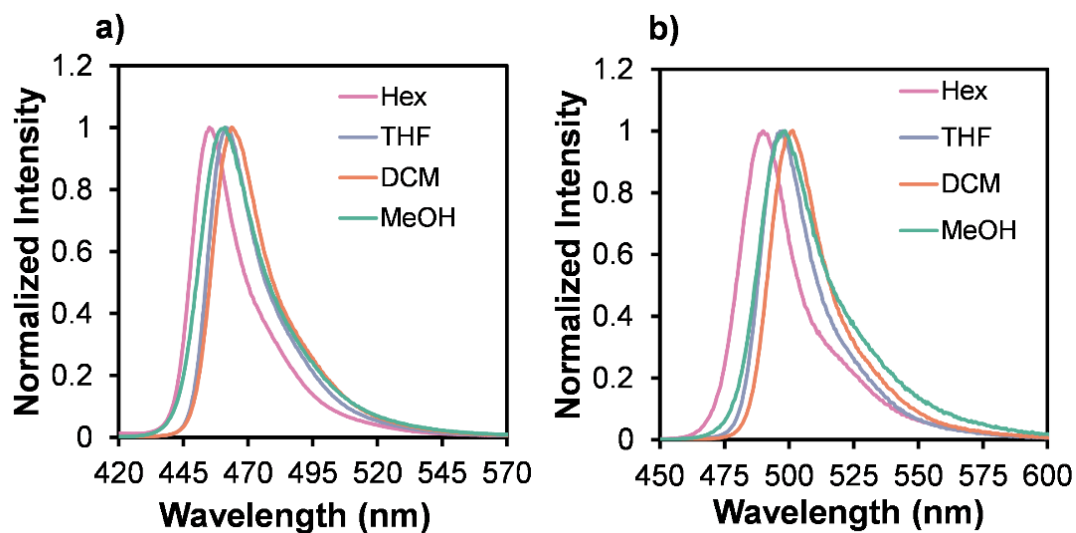


Figure S16. PL spectra of a) NBOPO, and b) NBNPO at room temperature in different solvents (3×10^{-5} M).

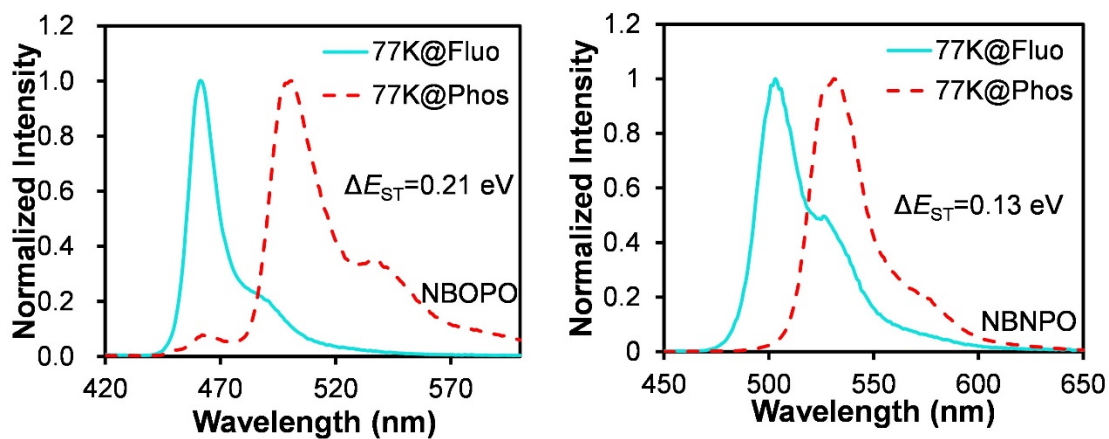


Figure S17. The fluorescence and phosphorescence spectra of NBOPO (left) and NBNPO (right) in toluene at 77 K.

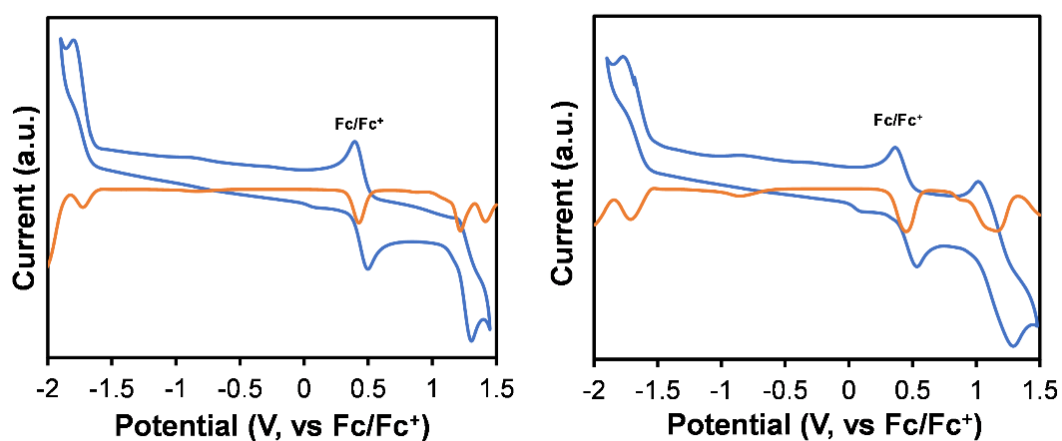


Figure S18. Cyclic voltammograms and differential pulse voltammetry curves for NBOPO (left) and NBNPO (right). The curves were measured at room temperature with 0.1 M solution of $n\text{-Bu}_4\text{NPF}_6$ in CH_2Cl_2 for the reduction and the oxidation scan (vs Fc/Fc^+); HOMO and LUMO energies obtained from electrochemical data.

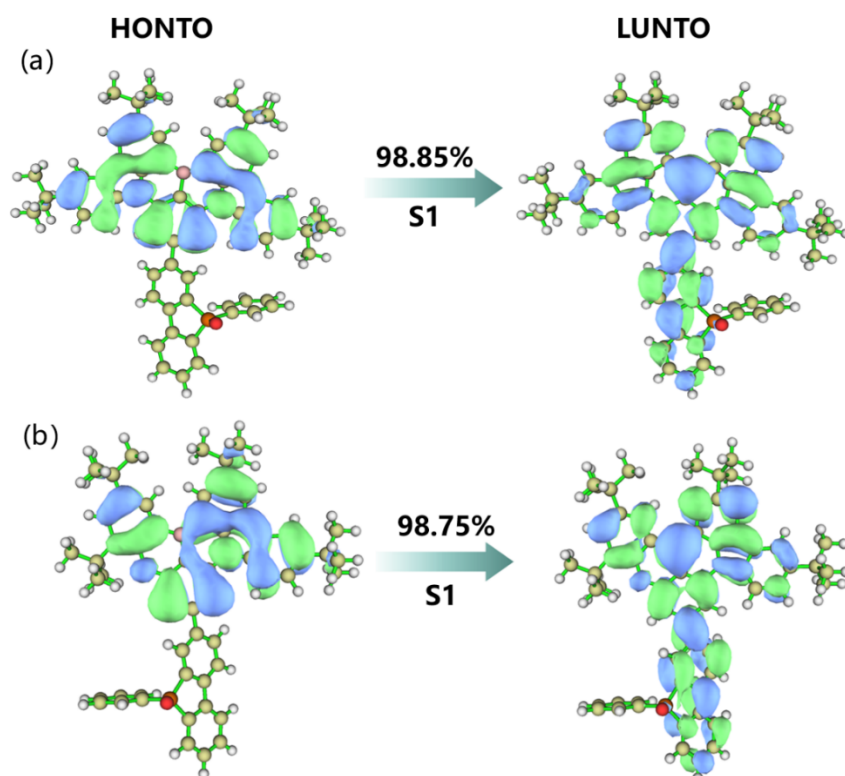


Figure S19. Natural transition orbitals (NTOs) describing the excitation characters of the S1 state in (a) NBNPO (b) NBOPO: the weights of the NTO pair with the highest contributions to the excitations are included. For these two compounds, the transition of the S1 state is predominantly dominated by π to π^* transitions.

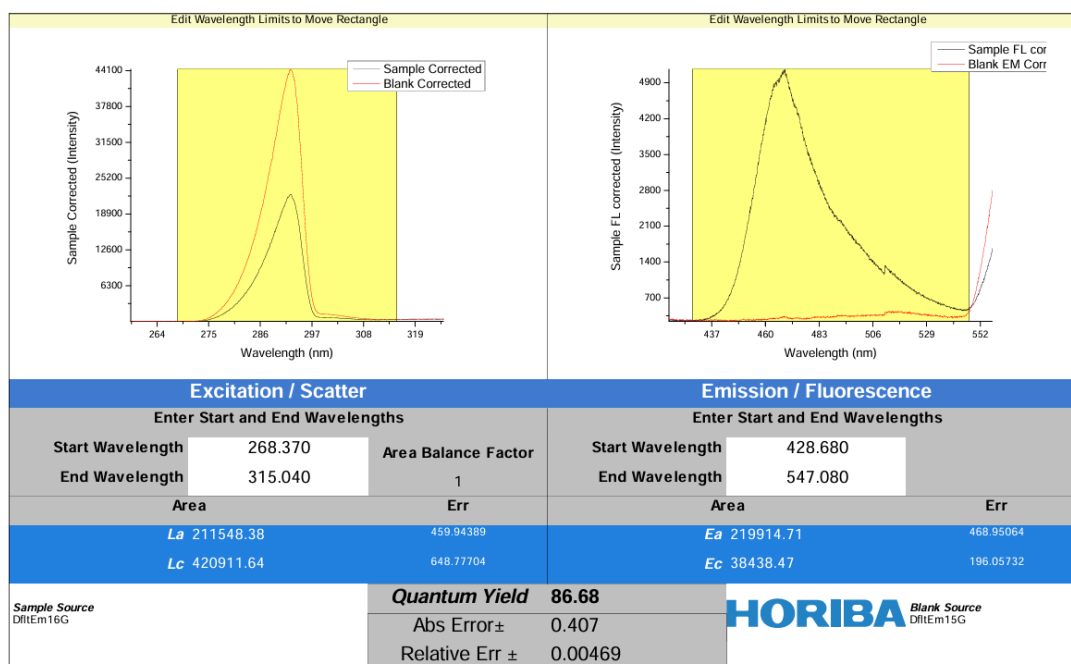


Figure S20. PLQY of NBOPO in doped film (5 wt%).

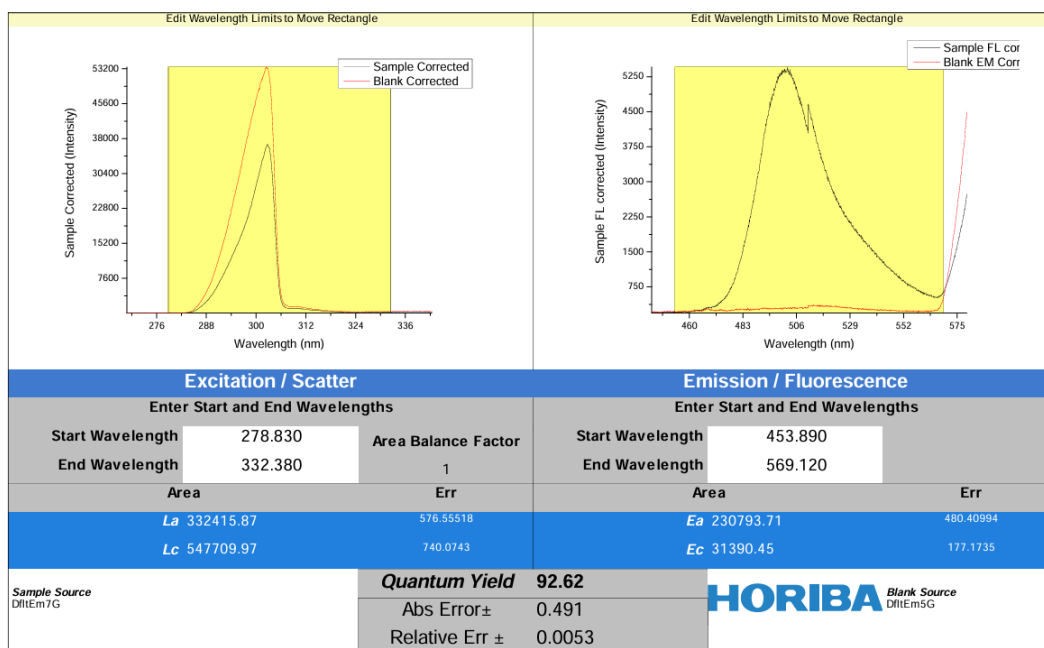


Figure S21. PLQY of NBNPO in doped film (5 wt%).

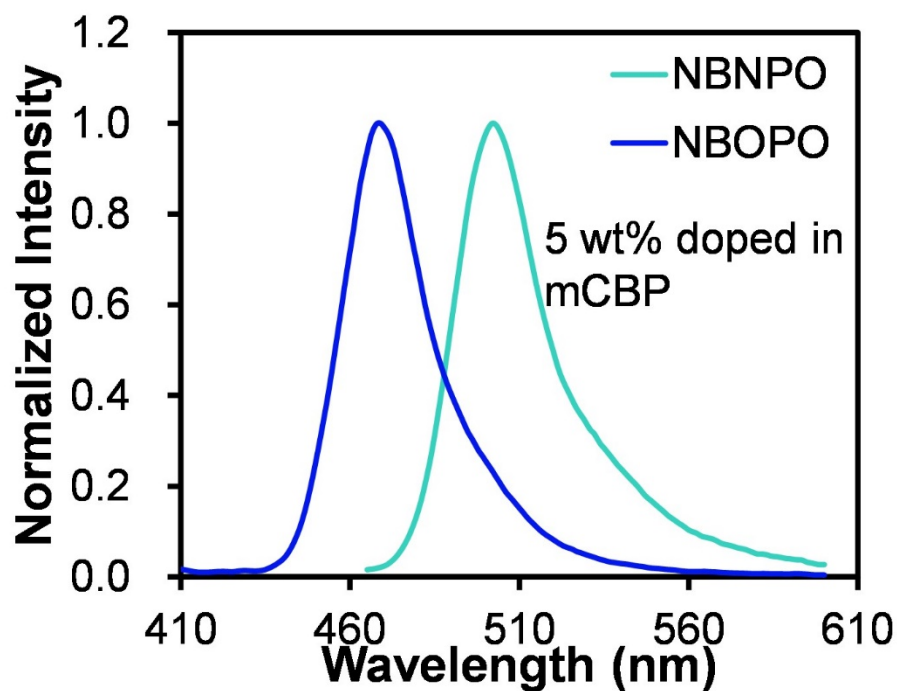


Figure S22. The measured PL spectra of 5 wt% NBOPO and NBNPO doped in mCBP host at room temperature.

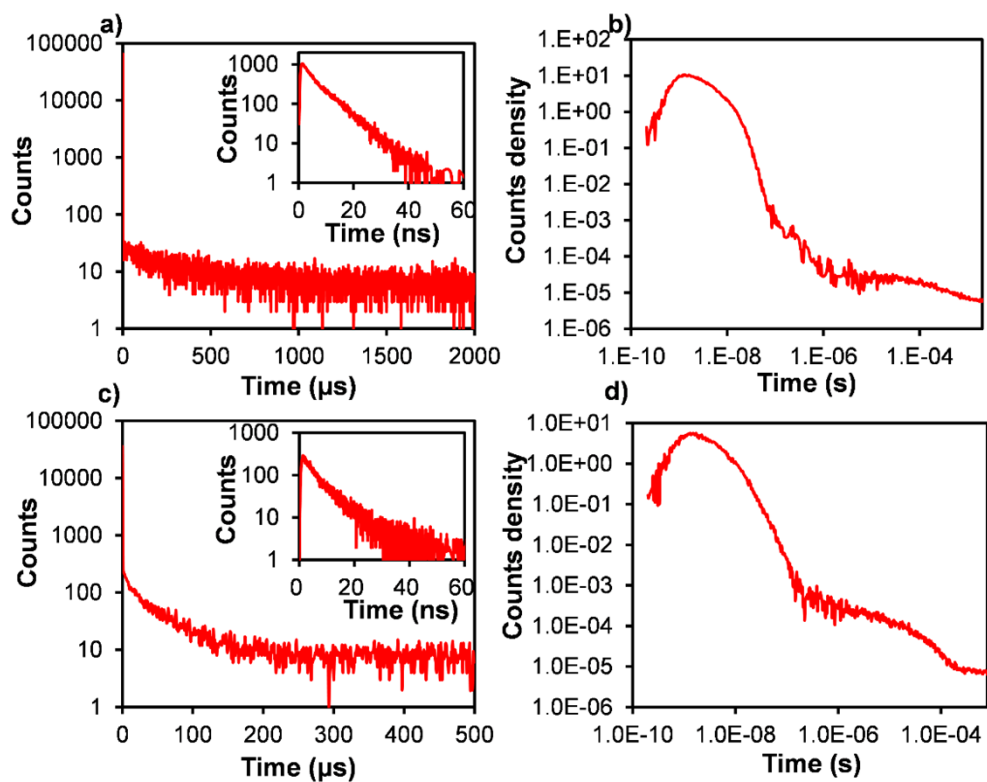


Figure S23. The transient PL prompt and decay curves of a), b) NBOPO and c), d) NBNPO doped in the host at room temperature (5 wt%).

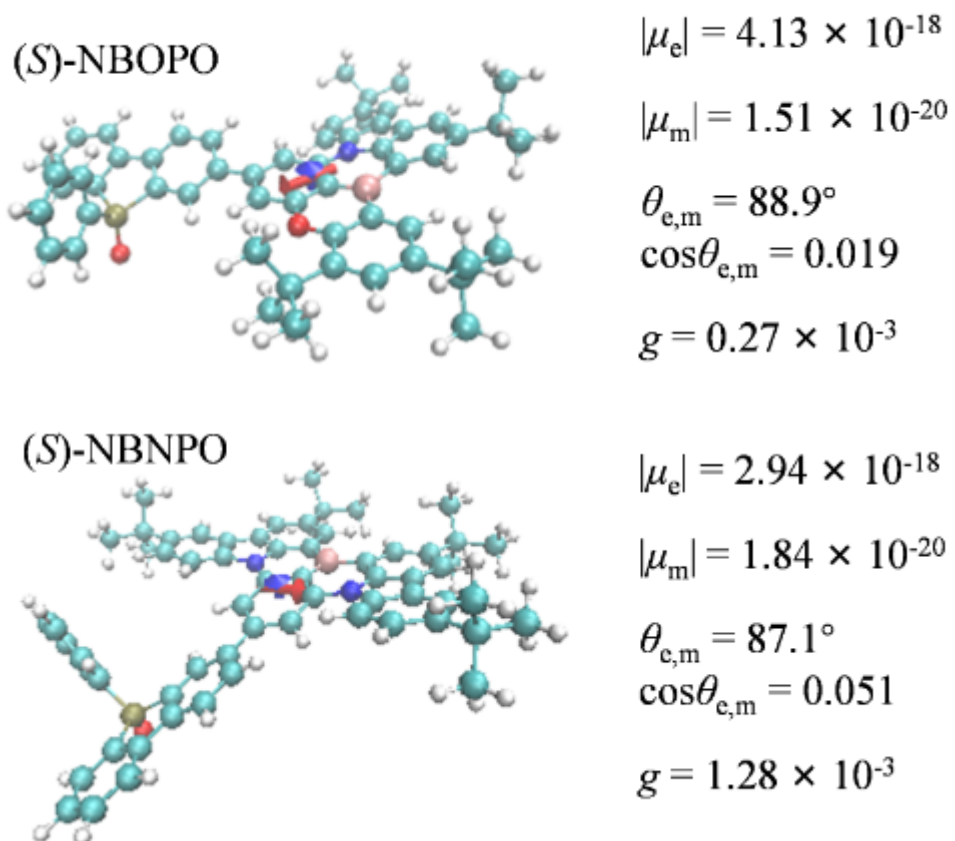


Figure S24. Simulated electronic transition dipoles (μ_e , red), magnetic transition dipoles (μ_m , blue), $\cos\theta_{e,m}$ and calculated g values.

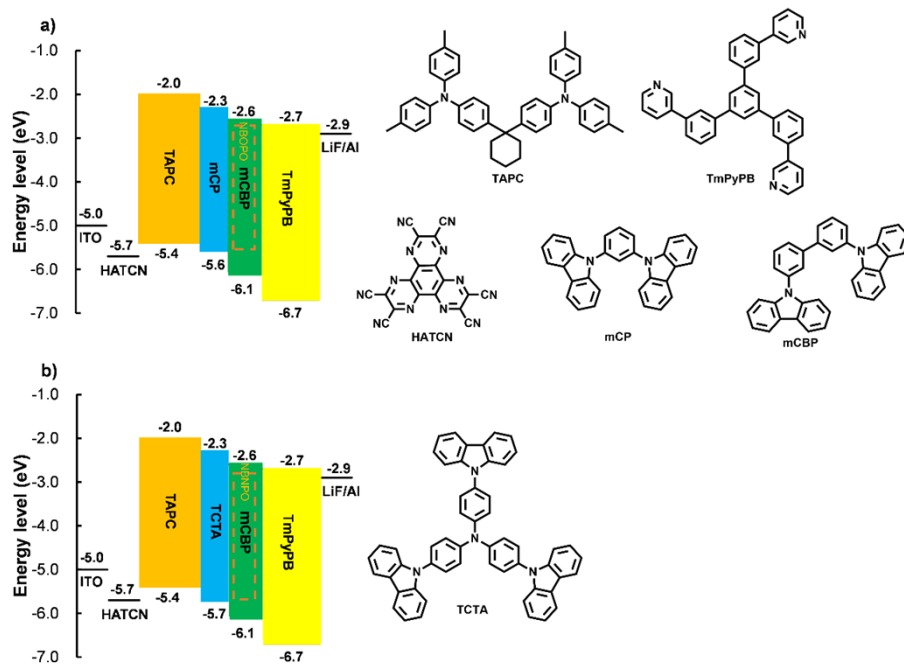


Figure S25. Structure and energy diagrams of CP-OLEDs of a) (*R/S*)-NBOPO and b) (*R/S*)-NBNPO.

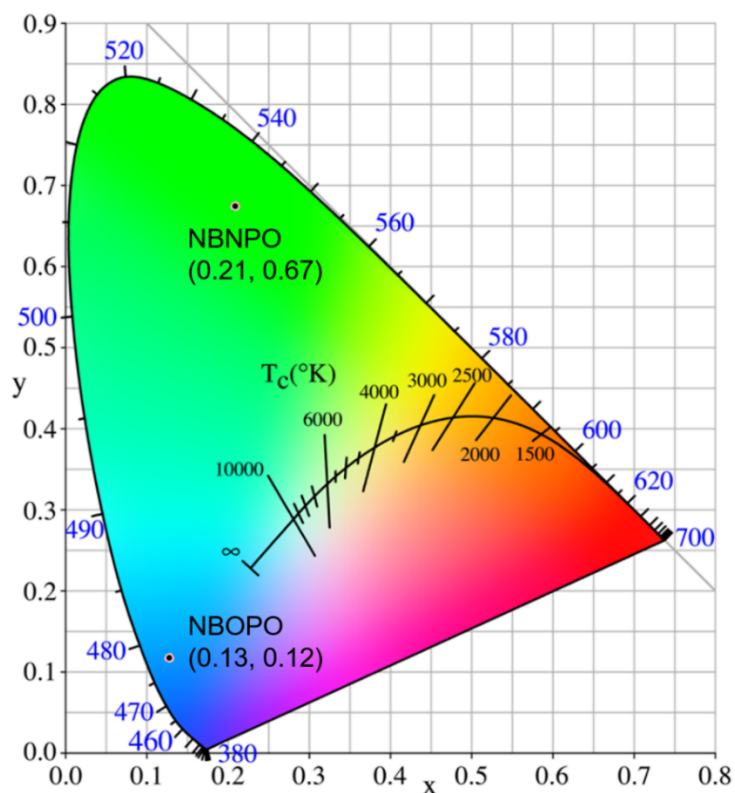


Figure S26. The corresponding CIE coordinates of (*R*)-NBOPO and (*R*)-NBNPO in OLEDs.

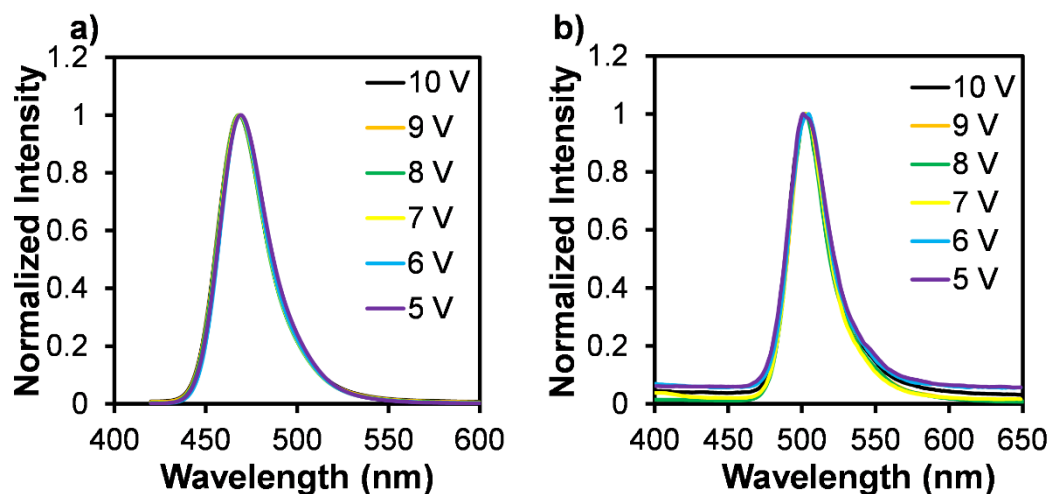


Figure S27. EL spectra of a) (R)-NBOPO and b) (R)-NBNPO device at different voltages

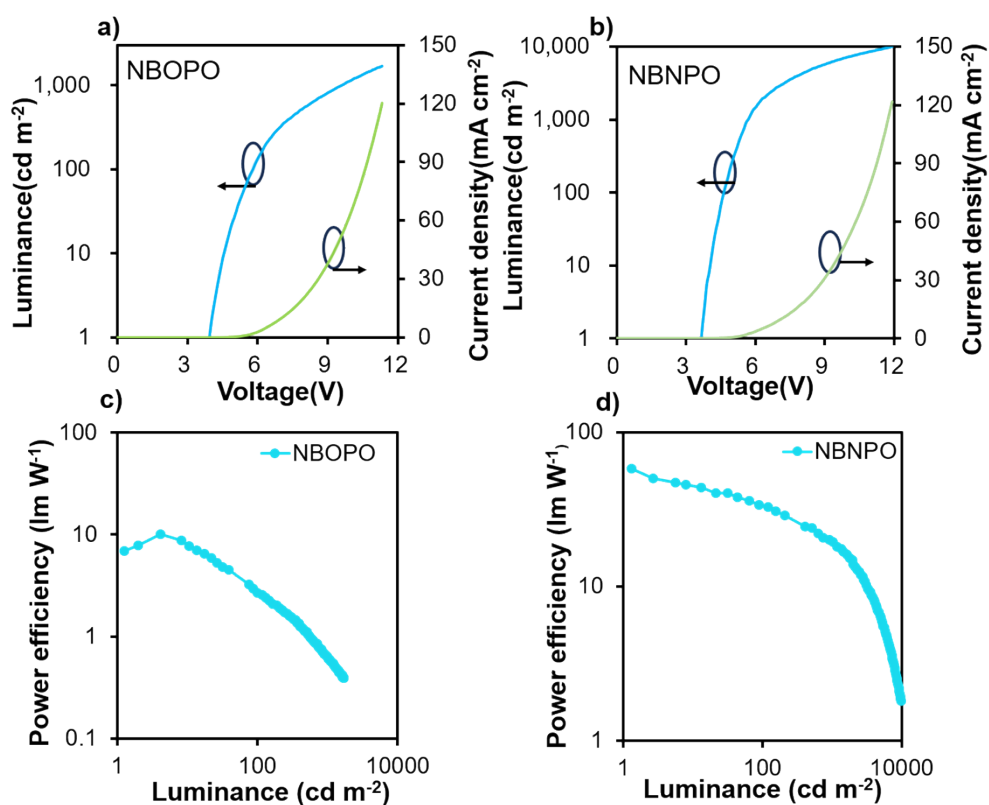


Figure S28. Luminance and current density versus voltage curves of a) (R)-NBOPO and b) (R)-NBNPO; Power efficiency versus luminance curves of c) (R)-NBOPO and d) (R)-NBNPO

Table S2. TD-DFT calculated electronic transitions for NBOPO along with their corresponding excitation energies and oscillator strengths.

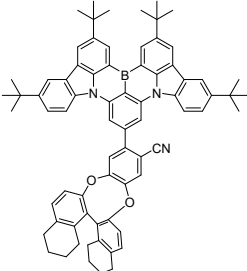
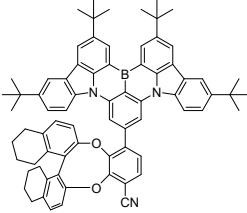
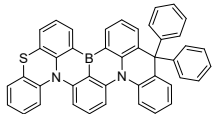
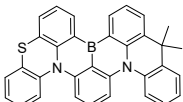
Compound	Spin State	Transition Configuration	Excitation Energy [nm (eV)]	Oscillator Strength
NBOPO	S ₁	HOMO→LUMO (94%)	413.44 (3.00)	0.3725
		HOMO→LUMO+1 (5%)		
	S ₂	HOMO→LUMO (5%)	353.50 (3.51)	0.0503
		HOMO→LUMO+1 (91%)		
	S ₃	HOMO-3→LUMO (2%)	343.52 (3.61)	0.0326
		HOMO-2→LUMO (6%)		
		HOMO-1→LUMO (83%)		
		HOMO-1→LUMO+1 (5%)		
	S ₄	HOMO-3→LUMO (23%)	333.88 (3.71)	0.9217
		HOMO-3→LUMO+1 (4%)		
		HOMO-2→LUMO (61%)		
		HOMO-1→LUMO (8%)		
	S ₅	HOMO-3→LUMO (64%)	330.04 (3.76)	0.1141
		HOMO-2→LUMO (24%)		
		HOMO-2→LUMO+1 (8%)		

Table S3. TD-DFT calculated electronic transitions for NBNPO along with their corresponding excitation energies and oscillator strengths.

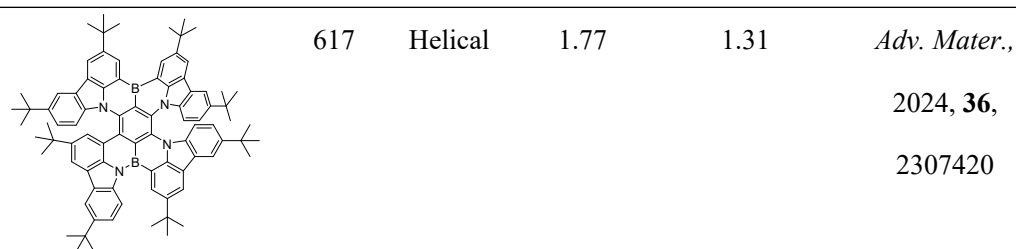
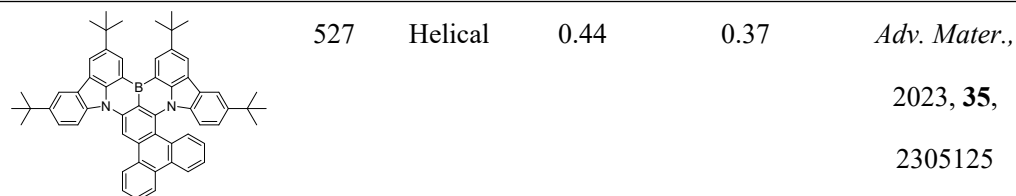
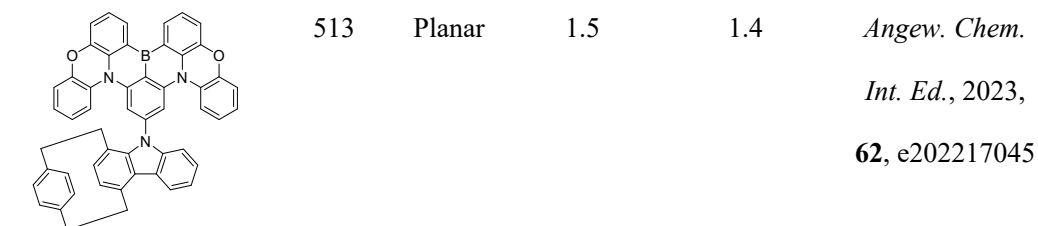
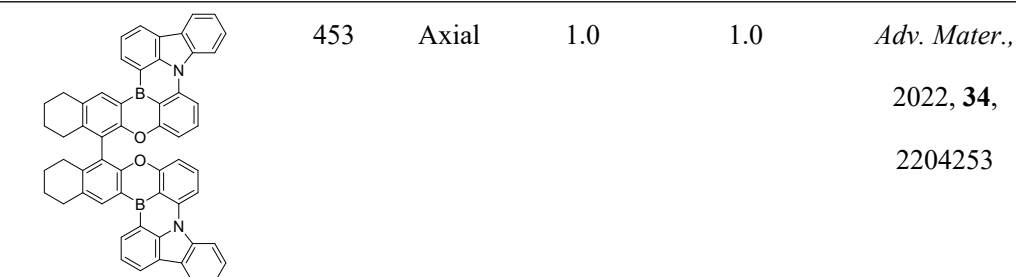
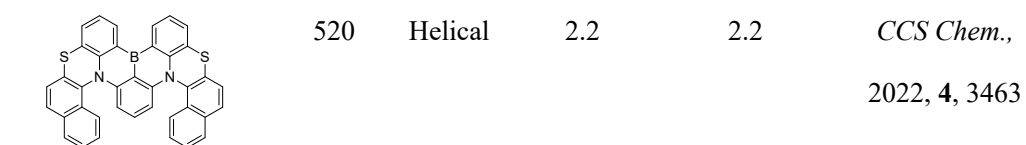
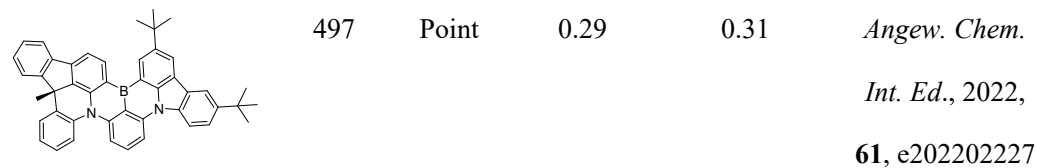
Compound	Spin State	Transition Configuration	Excitation Energy [nm (eV)]	Oscillator Strength
NBNPO	S ₁	HOMO→LUMO (96%)	447.90 (2.77)	0.4781
		HOMO→LUMO+1 (2%)		

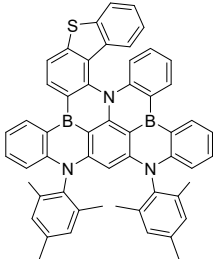
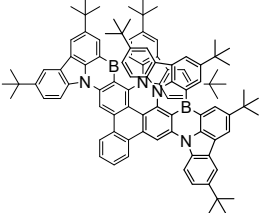
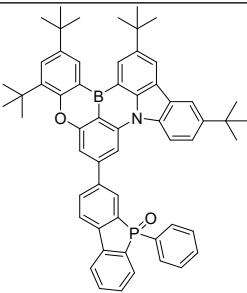
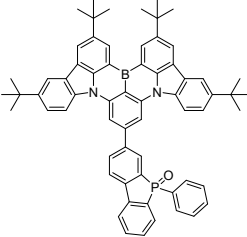
	S ₂	HOMO→LUMO (2%)	370.28 (3.35)	0.0475
		HOMO→LUMO+1 (94%)		
	S ₃	HOMO-1→LUMO (91%)	360.97 (3.43)	0.0283
		HOMO-1→LUMO+1 (3%)		
	S ₄	HOMO-3→LUMO (2%)	356.23 (3.48)	0.0106
		HOMO-2→LUMO (91%)		
		HOMO-2→LUMO+1 (3%)		
	S ₅	HOMO-4→LUMO (3%)	348.74 (3.56)	0.0476
		HOMO-3→LUMO (88%)		
		HOMO-2→LUMO (3%)		

Table S4. The photophysical and chiroptical performances of reported CP-MR-TADF materials.

Molecular structure	λ_{\max} (nm)	Chiral type	$ g_{EL} $ ($\times 10^{-3}$)	$ g_{PL} $ (doped film) ($\times 10^{-3}$)	Ref.
	493	Axial	1.43	0.91	<i>Adv. Mater.</i> , 2021, 33 , 2100652
	500	Axial	0.47	1.04	
	500	Helical	1.6	1.1	<i>Adv. Mater.</i> , 2022, 34 , 2105080
	497	Helical	3.1	1.3	<i>Adv. Mater.</i> , 2022, 34 ,

21050802



	444	Helical	0.26	1.1	<i>Adv. Mater.</i> , 2024, 36 , 2308314
	578	Helical	6.2	-	<i>Angew. Chem.</i> <i>Int. Ed.</i> , 2024, 63 , e202401835
	462	Point	1.4	1.18	
	498	Point	0.70	4.3	This work

Reference

1. M. J. Frisch, G. W. Trucks, H. B. Schlegel, G. E. Scuseria, M. A. Robb, J. R. Cheeseman, G. Scalmani, V. Barone, B. Mennucci, G. A. Petersson, H. Nakatsuji, M. Caricato, X. Li, H. P. Hratchian, A. F. Izmaylov, J. Bloino, G. Zheng, J. L. Sonnenberg, M. Hada, M. Ehara, K. Toyota, R. Fukuda, J. Hasegawa, M. Ishida, T. Nakajima, Y. Honda, O. Kitao, H. Nakai, T. Vreven, J. A. Montgomery, J. E. Peralta, F. Ogliaro, M. J. Bearpark, J. Heyd, E. N. Brothers, K. N. Kudin, V. N. Staroverov, R. Kobayashi, J. Normand, K. Raghavachari, A. P. Rendell, J. C. Burant, S. S. Iyengar, J. Tomasi, M. Cossi, N. Rega, N. J. Millam, M. Klene, J. E. Knox, J. B. Cross, V. Bakken, C. Adamo, J. Jaramillo, R. Gomperts, R. E. Stratmann, O. Yazyev, A. J. Austin, R. Cammi, C. Pomelli, J. W. Ochterski, R. L. Martin, K. Morokuma, V. G. Zakrzewski, G. A. Voth, P. Salvador, J. J. Dannenberg, S. Dapprich, A. D. Daniels, Ö. Farkas, J. B. Foresman, J. V. Ortiz, J. Cioslowski, D. J. Fox, *Gaussian 09 Revision C.01*, 2010.
2. T. Lu and F. Chen, *J. Comput. Chem.*, 2012, **33**, 580-592.

3. Y. Xu, C. Li, Z. Li, J. Wang, J. Xue, Q. Wang, X. Cai and Y. Wang, *CCS Chemistry*, 2022, **4**, 2065-2079.
4. S. Cai, G. S. M. Tong, L. Du, G. K. M. So, F. F. Hung, T. L. Lam, G. Cheng, H. Xiao, X. Chang, Z. X. Xu and C. M. Che, *Angew. Chem. Int. Ed.*, 2022, **61**, e202213392.
5. K. Baba, M. Tobisu and N. Chatani, *Angew. Chem. Int. Ed.*, 2013, **52**, 11892-11895.